LETTERS
https://doi.org/10.1038/s42255-019-0033-z

nature metabolism

Corrected: Author Correction

Olfaction regulates organismal proteostasis and longevity via microRNA-dependent signalling

Fabian Finger[1], Franziska Ottens[1], Alexander Springhorn[1], Tanja Drexel[2], Lucie Proksch[1], Sophia Metz[1], Luisa Cochella[2] and Thorsten Hoppe[1]*

The maintenance of proteostasis is crucial for any organism to survive and reproduce in an ever-changing environment, but its efficiency declines with age[1]. Post-transcriptional regulators such as micrRNAs (miRNAs) control protein translation of target mRNAs, with major consequences for development, physiology and longevity[2,3]. Here we show that food odour stimulates organismal proteostasis and promotes longevity in *Caenorhabditis elegans* through miR-71-mediated inhibition of *tir-1* mRNA stability in olfactory AWC neurons. Screening a collection of miRNAs that control ageing[3], we found that the miRNA miR-71 regulates lifespan and promotes ubiquitin-dependent protein turnover, particularly in the intestine. We show that miR-71 directly inhibits the Toll-receptor-domain protein TIR-1 in AWC olfactory neurons and that disruption of miR-71–*tir-1* or loss of AWC olfactory neurons eliminates the influence of food source on proteostasis. miR-71-mediated regulation of TIR-1 controls chemotactic behaviour and is regulated by odour. Thus, odour perception influences cell-type-specific miRNA–target interaction, thereby regulating organismal proteostasis and longevity. We anticipate that the proposed mechanism of food perception will stimulate further research on neuroendocrine brain-to-gut communication and may open the possibility for therapeutic interventions to improve proteostasis and organismal health via the sense of smell, with potential implications for obesity, diabetes and ageing.

MiRNA biogenesis is associated with improved stress tolerance and longevity in *C. elegans*[4], and specific miRNAs have been linked to stress resistance and ageing[3]. Changes in stress resistance and longevity are often associated with alterations in protein homeostasis (proteostasis)[1]. To identify miRNAs that control longevity via effects on organismal proteostasis, we used established in vivo assays to monitor ubiquitin-mediated turnover of fluorescently labelled model substrates in *C. elegans*[5,6]. The UbV-GFP protein is a ubiquitously expressed ubiquitin fusion degradation (UFD) substrate. In wild-type worms, polyubiquitination of the N-terminal ubiquitin moiety triggers degradation of UbV-GFP by the 26S proteasome. Disruption of ubiquitination or of proteasomal turnover resulted in UbV-GFP stabilization in transgenic worms (Fig. 1a)[5]. We also monitored endoplasmic reticulum (ER)-associated protein degradation (ERAD) by following the turnover of an unstable form of the cathepsin L–like cysteine protease CPL-1 (CPL-1*-YFP) expressed in intestinal cells[6]. CPL-1*-YFP was normally retrotranslocated out of the ER lumen for ubiquitin-mediated proteasomal degradation in the cytosol; loss of the ERAD-associated E3 ubiquitin–protein ligase SEL-1 triggered substrate stabilization[7] (Supplementary Figs. 1f and 3d).

Of the miRNA loss-of-function mutants we tested, we found that *mir-71(n4115)* worms, compared with wild-type worms, showed a substantially higher levels of both UbV-GFP and CPL-1*-YFP, particularly within the intestine (Fig. 1b,c and Supplementary Fig. 1a,g). Importantly, the levels of ubiquitination-resistant $^{K29/48R}$UbV-GFP and GFP were unaltered in *mir-71(n4115)* worms[5] (Supplementary Fig. 1b), and wild-type and *mir-71(n4115)* animals showed comparable levels of *UbV-GFP* mRNA (Supplementary Fig. 1c). Overexpression of the proteasomal subunit RPN-6.1, which triggers degradation of ubiquitinated proteins[8], suppressed the stabilization of UbV-GFP in *mir-71(n4115)* animals (Supplementary Fig. 1d). In contrast, loss of the E3 ligase HECD-1, which acts upstream of the 26S proteasome in substrate ubiquitination, was not compensated for by elevated RPN-6.1 levels (Supplementary Fig. 1d)[5]. RNA interference (RNAi)-mediated knockdown of *hecd-1*, as well as *rpn-8*, led to an additive defect when combined with the *mir-71(n4115)* allele (Supplementary Fig. 1e). These data suggest that miR-71 regulates ubiquitin-dependent protein degradation via the 26S proteasome.

Consistently with ERAD defects, *mir-71(n4115)* worms are sensitive to ER stress induced by tunicamycin (TM), which blocks N-linked glycosylation of ER proteins[9]. Interestingly, the lifespan of *mir-71(n4115)* worms, which was previously reported to be reduced[3], was further shortened by TM treatment (Supplementary Fig. 1i). To further characterize the role of miR-71 in intestinal proteostasis, we performed tissue-specific rescue experiments[10]. Ubiquitous and pan-neuronal, but not hypodermal, expression of *mir-71* in *mir-71(n4115)* worms rescued the defective turnover of UbV-GFP (Supplementary Fig. 2a,b). These data suggest that loss of *mir-71* expression in neurons stabilizes UbV-GFP in intestinal cells. Previous work has revealed that *mir-71* is expressed in olfactory neurons[11]. To identify the type of neuron required for miR-71-dependent regulation of proteostasis, we genetically abolished the specification of AWA; AWB and ADF; AWC; or PQR, PHA and PHB olfactory neurons by depleting the transcription factors required for their cell-fate determination: ODR-7, LIM-4, CEH-36 and CEH-14, respectively[12]. Abrogation of either AWB and ADF (*lim-4*) or AWC (*ceh-36*) development partially suppressed UbV-GFP accumulation in *mir-71(n4115)* worms (Supplementary Fig. 2c), thus suggesting that these olfactory neurons are required for miR-71-mediated regulation of intestinal homeostasis. Intriguingly, the AWCs belong to a class of ciliated olfactory neurons previously implicated in the regulation of longevity[13]. This finding led us to hypothesize a prominent role of AWC neurons in organismal proteostasis via miR-71.

To test this hypothesis, we first confirmed that *mir-71* is expressed in AWC neurons. Indeed, we observed colocalization

[1]Institute for Genetics and CECAD Research Center, University of Cologne, Cologne, Germany. [2]Research Institute of Molecular Pathology (IMP), Vienna BioCenter (VBC), Vienna, Austria. *e-mail: thorsten.hoppe@uni-koeln.de

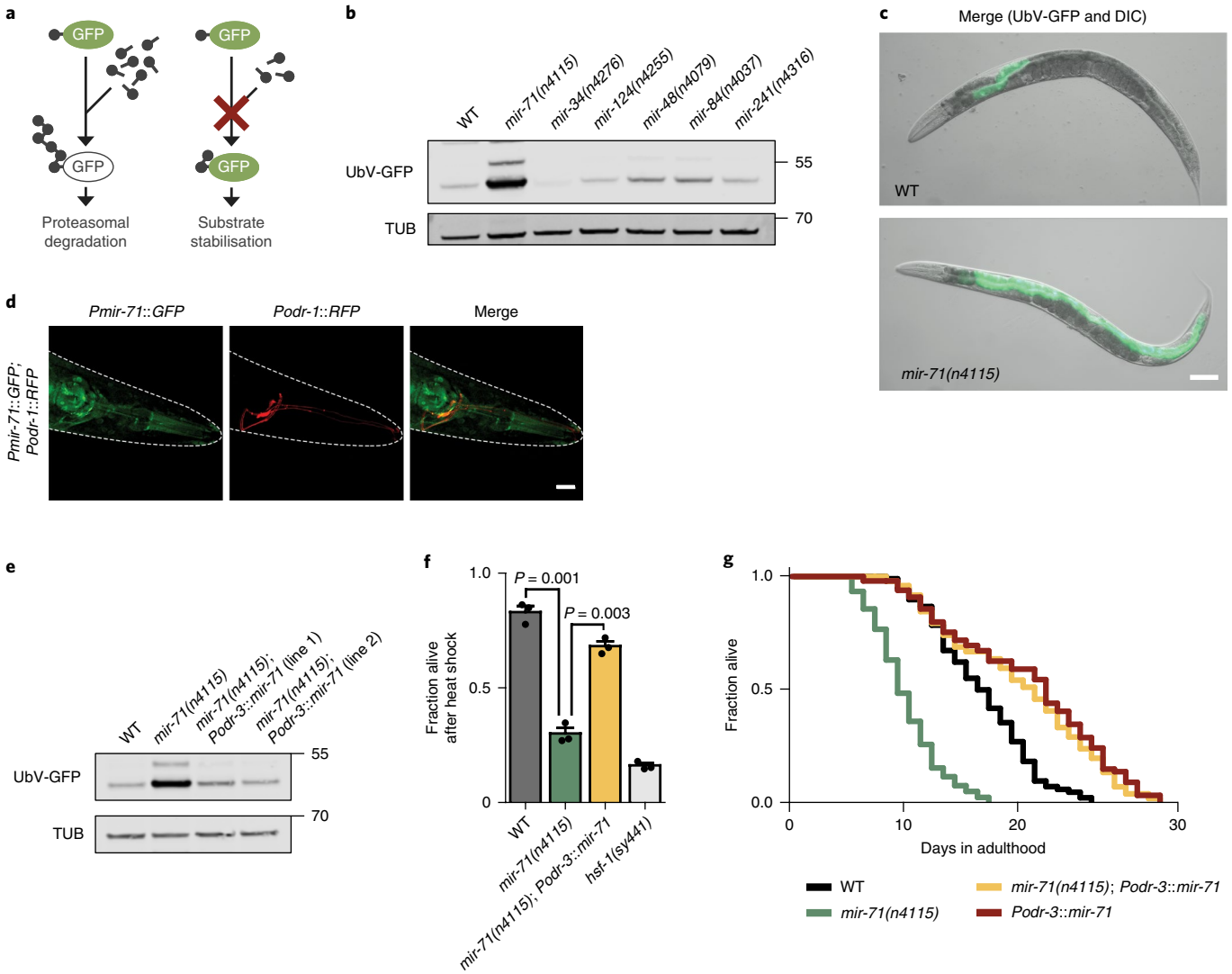

Fig. 1 | Expression of *mir-71* in olfactory neurons supports proteostasis and longevity. a, The UFD model substrate for monitoring ubiquitin-dependent degradation. **b**, Worms with the *mir-71(n4115)* deletion allele exhibited stabilization of the UFD substrate. Detection of GFP signal was done via western blotting showing UbV-GFP and tubulin (TUB) levels. WT, wild type. **c**, The UFD substrate accumulated mainly in the intestine with *mir-71(n4115)* deletion. Representative fluorescence images are shown of day 1 adult worms with the indicated genotypes. Merge shows UbV-GFP and differential interference contrast (DIC) images. Scale bar, 250 µm. **d**, *mir-71* is expressed in olfactory (AWC) neurons. Confocal microscopy images show localization of GFP expressed from *Pmir-71::GFP* (green) and AWC neurons (red). Scale bar, 15 µm. **e**, AWC-selective rescue of the *mir-71(n4115)*-deletion mutant restores protein degradation. Western blots are of day 1 adult worm lysates with the indicated genotypes, showing UbV-GFP and tubulin levels. **f**, AWC-selective expression of *mir-71* increases survival after heat stress. The *hsf-1(sy441)* mutant served as a stress-sensitive control. Bars show mean values ± s.e.m. obtained from $n = 3$ biological replicates using at least 50 worms (mean values represented by dots); statistics determined by one-way analysis of variance (ANOVA) with post hoc test. **g**, AWC-selective expression of *mir-71* extends lifespan. Statistics details can be found in Supplementary Table 1. In **b**–**e**, representative data were derived from at least three independent experiments yielding similar results. In **b** and **e**, molecular weights are shown in kilodaltons (kDa).

of GFP expressed from the *mir-71* promoter (*Pmir-71*::*GFP*) and RFP expressed from the promoter of the AWC-specific marker *odr-1* (*Podr-1*::*RFP*)[11] (Fig. 1d). Furthermore, *Podr-1*::*RFP* expression revealed comparable AWC neuronal integrity in *mir-71(n4115)* and wild-type worms (Supplementary Fig. 2d). Intriguingly, selective expression of *mir-71* in AWC (*odr-3* promoter) but not AWB (*str-1* promoter) neurons fully restored the ability of *mir-71(n4115)* animals to degrade UbV-GFP[14] (Fig. 1e and Supplementary Fig. 2e,f). AWC-selective expression of *mir-71* in *mir-71(n4115)* worms alleviated mortality induced by the proteasome inhibitor bortezomib (BTZ) (Supplementary Fig. 2g) as well as heat sensitivity, and reduced lifespan (Fig. 1f,g). Further, *Podr-3*::*mir-71* expression prolonged the lifespan of wild-type worms (Fig. 1g), thereby suggesting that miR-71 improves organismal physiology. Thus, *mir-71* expression in AWC olfactory neurons is necessary and sufficient to coordinate organismal proteostasis, particularly in the intestine.

MiRNAs regulate gene expression via complementary base-pairing with target mRNAs. To identify potential targets of miR-71 important for proteostasis regulation, we compiled a list of genes that were differentially expressed in olfactory neurons (i) after proteasomal inhibition of wild-type worms and (ii) in the *mir-71(n4115)*-deletion mutant, relative to wild-type worms (Supplementary Fig. 3a and Supplementary Table 2). We further reduced the list to AWC-specific mRNAs regulated in response to proteotoxic stress, on the basis of RNA sequencing data and bioinformatic miRNA-target prediction (Fig. 2a and Supplementary Table 3) (TargetScanWorm release 6.2)[15].

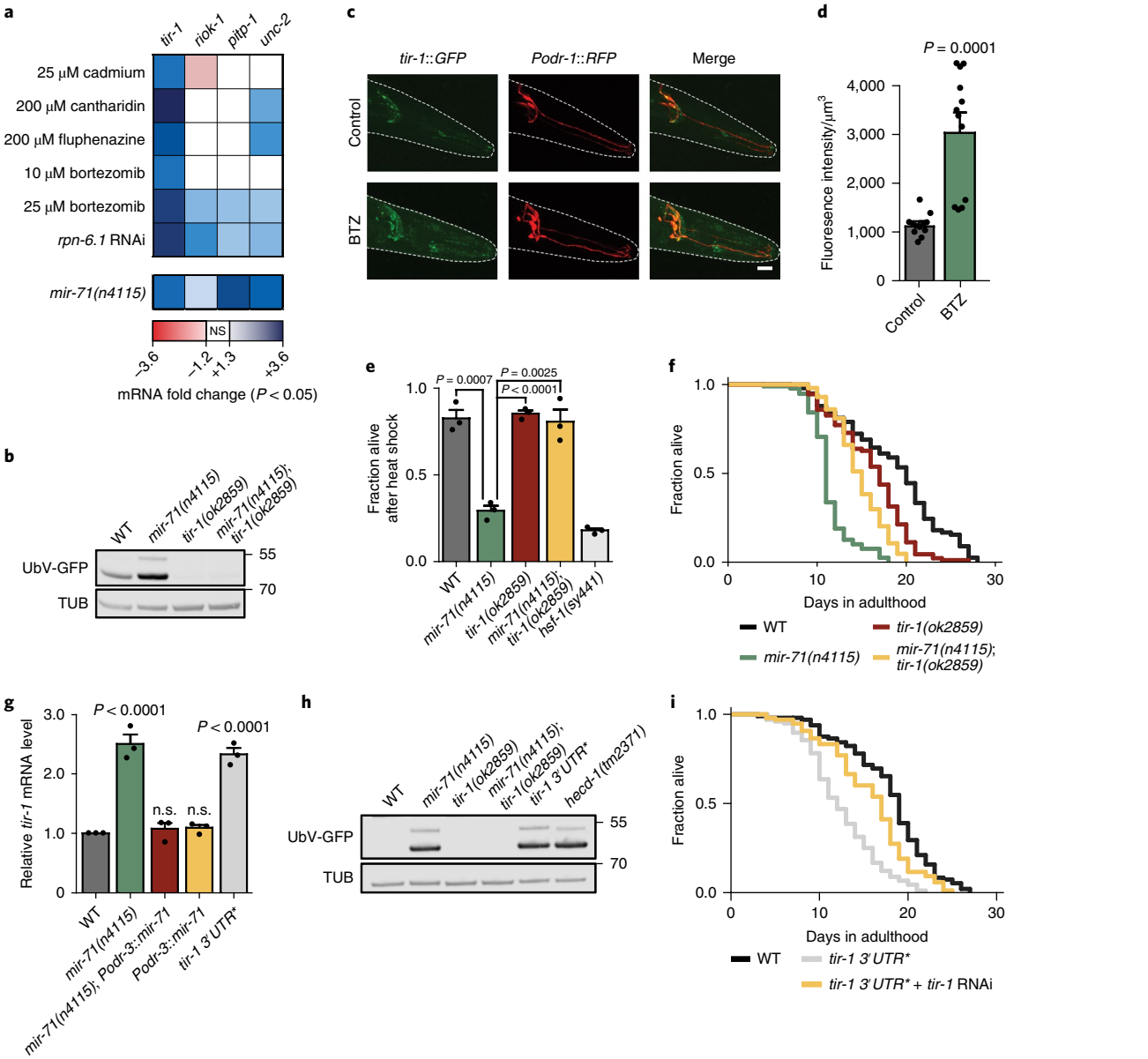

Fig. 2 | Negative regulation of *tir-1* by miR-71 is important for proteostasis and longevity. a, mRNA levels of predicted miR-71 targets (TargetScanWorm release 6.2). Color-coded transcriptional responses of mRNAs expressed in AWC neurons are shown under multiple proteotoxic stress conditions or in the *mir-71(n4115)*-deletion mutant. Expression levels are relative to those of untreated wild-type worms and were determined via RNA sequencing (top) ($n = 3$ biological replicates) or microarray (bottom) ($n = 4$ biological replicates); NS, not significant. **b**,**h**, Representative western blots from day 1 adult worms of the indicated genotypes, showing UbV-GFP and tubulin levels. Data were derived from at least three independent experiments with similar results. Molecular weights (kDa) are shown. **b**, *tir-1(ok2859)* deletion suppresses *mir-71(n4115)*-induced proteolytic defects. **c**, Proteotoxic stress increases TIR-1 levels in AWC neurons. Confocal microscopy images show expression from *tir-1*::*GFP* (green) and AWC neurons (red). Scale bar, 15 μm. **d**, Quantification of the TIR-1::GFP fluorescence intensity shown in **c**. Dimethyl sulfoxide (DMSO) was used as a solvent control but did not show a significant difference relative to the control condition (1,322.24 ± 96.05; data not shown). Bars show mean values ± s.e.m. obtained from $n = 12$ individual animals (represented by dots). Statistics were determined by one-way ANOVA with post hoc test. **e**, Heat-stress sensitivity of the *mir-71(n4115)* mutant is suppressed by *tir-1(ok2859)* deletion. The *hsf-1(sy441)* mutant served as a control. Bars show mean values ± s.e.m. obtained from $n = 3$ biological replicates with at least 50 worms (mean values represented by dots); statistics were determined by one-way ANOVA with post hoc test. **f**, *tir-1(ok2859)* deletion extends the lifespan of *mir-71(n4115)* worms. Statistical details can be found in Supplementary Table 1. **g**, miR-71 negatively regulates *tir-1* transcript levels. Relative *tir-1* mRNA levels were measured by quantitative real-time PCR in day 1 adult worms. Data were normalized to values for wild-type worms. Bars show mean values ± s.e.m. obtained from $n = 3$ biological replicates with 3 technical replicates each (mean values represented by dots); statistics were determined by one-way ANOVA with post hoc test. **h**, AWC-selective expression of *mir-71* does not suppress proteostasis defects caused by the *tir-1 3′UTR** mutation. **i**, The *tir-1 3′UTR** mutation shortens lifespan. Statistical details can be found in Supplementary Table 1.

We identified *tir-1*, *riok-1*, *pitp-1* and *unc-2* as potential targets of miR-71. In particular, *tir-1* mRNA was strongly elevated in response to proteotoxic reagents and contains three predicted miR-71-binding sites within the 3′ untranslated region (UTR; Fig. 2a, Supplementary Fig. 3a, and Supplementary Tables 2 and 3). To test whether upregulation of the identified genes might account for the

defects in proteostasis of *mir-71*-deficient animals, we depleted the candidate mRNAs by RNAi. Only *tir-1* depletion restored UbV-GFP levels in *mir-71(n4115)* mutants (Supplementary Fig. 3b). Furthermore, degradation of both the UFD and ERAD substrates was restored in *mir-71(n4115)*; *tir-1(ok2859)* double mutants (Fig. 2b and Supplementary Fig. 3c,d). Finally, ubiquitination-resistant $^{K29/48R}$UbV-GFP and GFP proteins, as well as *UbV-GFP* mRNA levels, were unaltered in *tir-1(ok2859)* worms (Supplementary Fig. 3e,f), thus revealing that the decrease in substrate protein levels did not result from transcriptional or translational changes.

TIR-1 is a Toll-receptor-domain adaptor protein that is important for innate immune responses and neuronal development[11,16,17]. To determine where *tir-1* was expressed, we used CRISPR–Cas9-based gene editing to generate a *tir-1*::*GFP* reporter. We observed TIR-1::GFP expression in AWC olfactory neurons[11,16]. Furthermore, proteotoxic stress via BTZ treatment increased the expression of TIR-1::GFP as well as *tir-1* mRNA levels (Fig. 2a–d). Importantly, loss of *tir-1* suppressed the heat-stress sensitivity and shortened the lifespan of *mir-71(n4115)* mutants (Fig. 2e,f). We also evaluated a gain-of-function mutant, *tir-1(yz68)*, which has constitutive activation of TIR-1 (ref. [18]). In contrast to loss of TIR-1, the *tir-1(yz68)* mutation resulted in a slight increase in UbV-GFP levels, which further increased in the context of *mir-71(n4115)* deletion (Supplementary Fig. 3g,h). These findings suggest that miR-71 negatively regulates *tir-1*.

To test whether *tir-1* mRNA is a direct target of miR-71, we used a CRISPR–Cas9 approach to disrupt all three predicted miR-71-binding sites in an endogenous allele of *tir-1* in wild-type worms (*tir-1 3′UTR**) (Supplementary Fig. 4a). Indeed, *tir-1* mRNA levels increased in *tir-1 3′UTR** worms relative to wild-type worms (Fig. 2g, grey bar), thus indicating a direct repressive effect of the miRNA. Furthermore, the *mir-71(n4115)* deletion mutant showed increased levels of *tir-1* mRNA (Fig. 2g, green bar), in line with our microarray analysis results (Fig. 2a). Expression of *mir-71* in AWCs restored *tir-1* mRNA to wild-type levels in *mir-71(n4115)* worms, thereby demonstrating that the *tir-1* deregulation observed in *mir-71*-mutant animals occurs primarily in AWC neurons (Fig. 2g, red versus green bar).

Importantly, animals carrying the *tir-1 3′UTR** allele accumulated both UFD and ERAD substrates, fully mimicking the phenotype of *mir-71(n4115)*-related defects in protein degradation (Fig. 2h and Supplementary Fig. 4b–d). RNAi-mediated depletion of *tir-1* or overexpression of RPN-6.1 suppressed the protein-turnover defect in *tir-1 3′UTR** animals (Supplementary Fig. 4e,f). Thus, the substrate stabilization caused by *tir-1 3′UTR** depends on increased *tir-1* levels and results from ubiquitin–proteasome system (UPS) dysfunction. Overexpression of *mir-71* in AWC neurons did not re-establish UPS function in *tir-1 3′UTR** animals, thus highlighting the unique importance of *tir-1* mRNA regulation for proteostasis (Supplementary Fig. 4g). Similarly to loss of *mir-71*, loss of *tir-1 3′UTR** also decreased lifespan, and this effect was rescued by RNAi-mediated depletion of *tir-1* (Fig. 2i). These data suggest that miR-71–*tir-1* forms a one-to-one miRNA–mRNA interaction that regulates proteome stability and longevity.

We previously showed that feeding worms with different bacterial food sources modifies protein degradation in the intestine[5]. As expected, UbV-GFP was efficiently degraded in wild-type worms grown on standard food, *Escherichia coli* strain OP50, but accumulated in worms fed *E. coli* C600, HT115 or HB101 (Fig. 3a). In contrast, *mir-71(n4115)* mutants did not display food-related changes in ubiquitin-dependent proteolysis, but these differences were restored by AWC-selective *mir-71* expression (Fig. 3a,b and Supplementary Fig. 5a).

Similarly to *mir-71(n4115)* animals, *tir-1 3′UTR** animals exhibited high levels of UbV-GFP, irrespective of the different bacterial strains (Supplementary Fig. 5b). In contrast, *tir-1(ok2859)* loss-of-function mutants did not accumulate UbV-GFP when grown on HB101 bacteria, and this effect was reversed by AWC-selective *tir-1* expression (Fig. 3c and Supplementary Fig. 5b,c). We found that *UbV-GFP* and *tir-1* mRNA levels were higher when *Podr-3*::*tir-1* was expressed in *mir-71(n4115)* mutants compared with wild-type worms, a finding consistent with loss of miRNA-mediated *tir-1* suppression in *mir-71(n4115)* worms (Fig. 3d). These data suggest that food-related changes in proteostasis are mediated at least in part by miR-71-dependent, cell-type-specific regulation of *tir-1* in AWC olfactory neurons.

Cell-nonautonomous neuroendocrine signalling pathways have been shown to trigger organismal regulation of proteotoxic stress and quality control[19,20]. Because UbV-GFP accumulated mainly in the intestine after exposure to different bacteria or *mir-71* deletion, we tested whether AWC-selective *tir-1* regulation might be communicated to peripheral tissues by neuronal signalling. We used an UNC-13 mutant to evaluate the consequences of blocking neurotransmitter release from small clear vesicles (SCVs) and an UNC-31 mutant to block neuropeptide release from dense core vesicles (DCVs)[21,22]. We found that both *unc-13(e51)* and *unc-31(e168)* mutants showed suppressed substrate stabilization in response to feeding with HB101 bacteria (Supplementary Fig. 5a), through loss of miR-71 function (Supplementary Fig. 5d) and *tir-1 3′UTR** mutation (Fig. 3e), thus suggesting that neuronal signal transduction is important for AWC-dependent coordination of proteostasis in peripheral tissues.

To determine the signalling molecules that trigger cell-nonautonomous communication from the olfactory neurons to the intestine, we evaluated changes in the expression of neuropeptide genes in *mir-71(n4115)* mutants compared with wild-type worms[23] (Fig. 3f and Supplementary Table 4). We observed high upregulation of NLP-9 and NLP-14 in *mir-71(n4115)* worms (Fig. 3f). Furthermore, RNAi-mediated depletion of NLP-9 and NLP-14 partially and fully suppressed *mir-71(n4115)*-dependent degradation defects, respectively (Fig. 3g). Thus, these data suggest that AWC neurons regulate intestinal homeostasis via secretion of the neuropeptides NLP-9 and NLP-14.

AWC neurons communicate with AIB and AIY interneurons, among others, and consequently initiate food- and odour-derived behaviour[24]. To validate the role of miR-71 in communication via the olfactory system, we analysed a loss-of-function mutant for *ttx-3*, which encodes a LIM-homeodomain protein necessary for AIY function[25]. Indeed, the *mir-71(n4115)*-dependent defects in protein degradation were suppressed in the *ttx-3(ot22)*-mutant background, thus supporting the idea that signal transduction via AIY interneurons connects food-derived olfactory inputs and proteostasis (Fig. 3h).

To define the cause of food-related changes in proteostasis, we monitored degradation of UbV-GFP in wild-type worms exposed to mixtures of OP50 and HB101 bacteria. In contrast to worms exposed to HB101 bacteria alone, worms raised on HB101:OP50 mixtures (100:1, 10:1 and 1:1) showed significantly decreased substrate stabilization almost indistinguishable from that of worms exclusively exposed to OP50 (Fig. 4a). However, *mir-71(n4115)* and *tir-1 3′UTR** worms did not distinguish between the different mixtures and showed UbV-GFP substrate stabilization, which in all cases did not exceed the effects seen with HB101 bacteria alone (Fig. 4a). The very low detection threshold for the proteostasis response to OP50 bacteria is consistent with the ability of *C. elegans* to detect low concentrations of volatile chemicals[26]. To acutely silence AWC activity specifically after development, we expressed a histamine-gated chloride channel (HisCl1) under the control of the *ceh-36* promoter and treated worms with histamine (HA; Supplementary Fig. 5e)[27]. Histamine treatment of worms grown on OP50 or HB101 bacteria completely abolished the food-evoked differences in UbV-GFP stabilization (Fig. 4b). Strikingly,

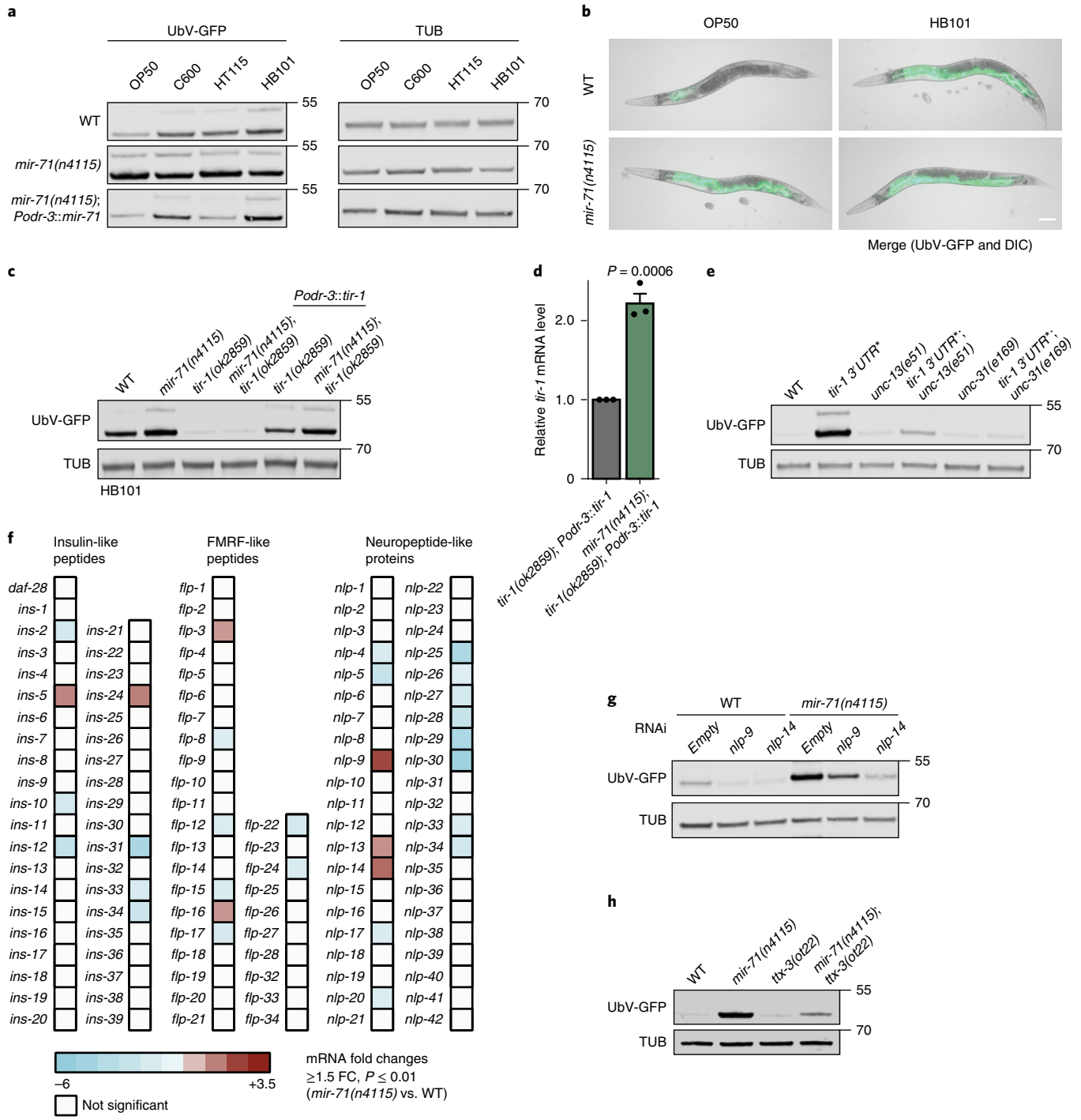

Fig. 3 | Food-dependent coordination of proteostasis is triggered by miR-71–*tir-1* dynamics in AWC neurons. a,**c**,**e**,**g**,**h**, Western blots of worm lysates with the indicated genotypes, showing UbV-GFP and tubulin levels. Data were derived from at least three independent experiments yielding similar results. Molecular weights (kDa) are shown. **a**, AWC-selective *mir-71* expression is important for food perception and proteostasis. Animals were grown on OP50, C600, HT115 or HB101 bacteria before worm lysis. **b**, Fluorescence images of day 1 adult worms grown on OP50 or HB101 bacteria with the indicated genotypes. Scale bar, 250 µm. Data were derived from at least three independent experiments yielding similar results. **c**, AWC-selective *tir-1* expression rescues food-dependent changes in protein degradation. Animals were grown on HB101 bacteria before worm lysis for western blotting. **d**, miR-71 negatively regulates *tir-1* transcript levels in AWC neurons. Relative *tir-1* mRNA levels were measured by quantitative real-time PCR in day 1 adult worms. Data were normalized to *tir-1(ok2859); Podr-3::tir-1*. Bars show mean values ± s.e.m. obtained from $n = 3$ biological replicates with 3 technical replicates each (mean values represented by dots); statistics were determined by two-tailed paired Student's *t* test. **e**, Neuronal signalling is required for changes in UPS activity caused by *tir-1 3′UTR**. **f**, Microarray data of *mir-71(n4115)* compared with wild-type worms reveals misregulation of neuropeptide expression. $n = 4$ biological replicates. FC, fold change. **g**, The NLP-9 and NLP-14 neuropeptides are important for proteostasis signalling of the *mir-71(n4115)* mutant. Representative western blots of worms treated with RNAi against the indicated factors, showing UbV-GFP and tubulin levels. **h**, Decreased AIY interneuron activity caused by *ttx-3(ot22)* suppresses the protein-degradation defects of *mir-71* deletion.

HA treatment similarly suppressed the degradation defects of *mir-71(n4115)* worms on both bacterial strains, thus suggesting a direct link between neuronal activity and miR-71 function in food-dependent regulation of proteostasis (Fig. 4c).

To discern the role of AWC neurons in smelling volatile odours, we used standard chemotaxis assays to test whether *tir-1* regulation is necessary for sensing a bacterial food source[28] (Fig. 4d). Indeed, both *mir-71(n4115)* and *tir-1 3′UTR** animals showed decreased food detection. The compromised chemosensation of *mir-71(n4115)* worms was rescued by *mir-71* expression in AWC but not AWB neurons (Fig. 4e and Supplementary Table 5). Similarly, the chemotaxis defects of *tir-1(ok2859)*-deletion animals were rescued by AWC-selective but not intestinal *tir-1* expression (Fig. 4f and Supplementary Table 5), thus suggesting that cell-type-specific *tir-1* regulation is required for both olfactory food perception and proteostasis. To test this hypothesis, we measured the levels of *tir-1* mRNA in wild-type worms exposed to the smell of bacteria. We incubated OP50 bacteria with aztreonam (Az), an antibiotic that affects bacterial cell division, thus resulting in inedible bacterial filaments (Fig. 4g)[29]. We found that *tir-1* mRNA levels increased in wild-type worms transferred to a plate without food, and the smell of inedible bacteria suppressed *tir-1* elevation in this context (Fig. 4h). Interestingly, *mir-71(n4115)* mutants, which already have upregulated *tir-1* mRNA, did not show a further increase in *tir-1* mRNA levels after transfer to a plate lacking food (Fig. 4i). These data suggest that the absence of an odour relieves miR-71-mediated repression of *tir-1* in wild-type worms. Our findings support a direct link between olfactory food perception and miR-71-mediated inhibition of TIR-1 to control proteostasis and ageing (Fig. 4j).

Previous reports indicated that neuroendocrine signalling communicates proteotoxic stress between neurons and the intestine[19,20]. However, little information has been gathered on the physiological roles of these systems. Given that proteostasis is linked to ageing and longevity[1], the olfactory system appears of particular importance, because food-derived volatile cues in *Drosophila melanogaster* and *C. elegans* affect lifespan[30,31]. Here we provide new mechanistic insights showing that a neuronal olfactory circuit rewires proteolytic networks in intestinal cells, thus establishing an underlying concept for the regulation of food adaption (Fig. 4j).

In this context, primary AWC olfactory neurons are central in sensing and transducing food-derived information. Interestingly, AWCs are OFF neurons, which exhibit high activity (intracellular Ca^{2+} levels) in the absence of food cues[24], a condition that results in gradual upregulation of *tir-1* mRNA (Fig. 4h) and might suggest a functional relationship between neuronal activity and *tir-1* abundance. In addition, *tir-1* is chronically upregulated in *mir-71(n4115)* mutants (Figs. 2a, 3d and 4i, and Supplementary Fig. 3a), thus indicating aberrant neuroendocrine signalling that interferes with stress tolerance, ageing and organismal proteostasis. Notably, TIR-1 is a Ca^{2+} signalling scaffold protein located near synapse structures important for proper AWC development[16] and adaptive chemotactic behaviour in neighbouring AWA neurons[32]. Together with our findings that *tir-1* levels are affected by food odour (Fig. 4h), this result might suggest far-reaching consequences for the underlying chemosensory circuits originating from AWCs. However, in-depth activity studies in AWCs and connected primary sensory neurons, as well as interneurons, will be needed to elucidate the precise role of TIR-1 within neuronal networks. Because we identified NLP-9 and NLP-14 as part of the miR-71–*tir-1*-dependent neuronal signalling towards the intestine (Fig. 3f,g), determining their exact origin and function, as well as respective receptors, will further aid in understanding the functionality of this cell-nonautonomous pathway.

The TIR-1 orthologue sterile-alpha- and armadillo-repeats-containing protein 1 (SARM1) is predominantly expressed in the mammalian brain and facilitates clearance of damaged axons in response to trauma or disease, a process also known as Wallerian degeneration. Mechanistically, the SARM1 TIR domain provides NADase activity, which triggers depletion of the essential metabolite NAD^+ and neuronal destruction[33]. Given that changes in NAD^+ levels are linked to proteasomal function, the NADase activity of SARM1 might directly affect ubiquitin-dependent protein degradation[34]. Here the TIR domain from *C. elegans* TIR-1 has a similar activity in axonal degeneration[35]. Interestingly, recent studies have further associated SARM1 with the development of nonalcoholic fatty liver disease induced by high-fat diet[36] as well as social interaction and cognitive flexibility in mice[37]. Together with our provided data on diet-dependent proteostasis and chemotactic behaviour, this finding might indicate evolutionarily conserved concepts of TIR-1/SARM1.

The perception of food-related odours might coordinate food appreciation and selection with physiological and metabolic demands of the digestive tract. In this context, it is interesting to note that *E. coli* OP50 and HB101 differ in their nutrient composition, with higher carbohydrate levels in HB101 bacteria. Consequently,

Fig. 4 | Coordination of food perception and organismal proteostasis. a–**c**, Western blots showing UbV-GFP and tubulin levels. Data were derived from at least three independent experiments yielding similar results. Molecular weights are shown in kDa. **a**, Low concentrations of OP50 alleviate HB101-dependent changes in proteostasis. Worms of the indicated genotypes were grown on the indicated mixtures of HB101 and OP50. **b**,**c**, AWC silencing by histamine-gated chloride channel expression (*Pceh-36::HisCl*). Food-dependent proteostasis defects in wild-type (**b**) and *mir-71(n4115)* (**c**) worms are inhibited after AWC silencing. Age-synchronized L4 larvae were grown on control (–) or HA-containing (10 mM HA) plates until day 1 of adulthood. **d**, Schematic overview of the chemotaxis assay: plates were separated into test and control quadrants. Worms were transferred to the centre of the plate. The number of animals in each quadrant was determined after 1.5 h. **e**,**f**, AWC-selective expression of *mir-71* (**e**) or *tir-1* (**f**) is important for chemotaxis behaviour (*E. coli* OP50). Chemotaxis assays were performed by using worms of the indicated genotypes. Bars show mean values ± s.e.m. obtained from $n = 9$ independent experiments (mean values represented by dots) with at least 66 (**e**) or 80 (**f**) animals. Statistics were determined by one-way ANOVA with post hoc test. **g**, *E. coli* treated with aztreonam (Az) showed abnormal cell growth and were not ingested by *C. elegans*. For an ingestion control, *E. coli* OP50 expressing GFP (OP50-GFP) were either treated with Az or left untreated before seeding into NGM plates. Worms were grown on the respective bacteria for 6 h before imaging. Fluorescence images are shown of day 1 adult worms. Scale bar, 250 µm. **h**,**i**, Food odour affects *tir-1* mRNA levels. Relative *tir-1* mRNA levels were measured in wild-type (**h**) and *mir-71(n4115)* (**i**) worms by quantitative real-time PCR in day 1 adult worms. Age-synchronized worms were grown on OP50 bacteria until day 1 of adulthood and transferred to plates without food (–) or with Az-treated OP50 (OP50 Az) for 1 or 4 h. Data were normalized to wild-type *tir-1* levels on food (control condition; data not shown). Bars show mean values ± s.e.m. obtained from $n = 3$ biological replicates with 3 technical replicates each (mean values represented by dots); statistics were determined by one-way ANOVA with post hoc test. **j**, Model: odours related to bacterial food are sensed via ciliated AWC olfactory neurons. The olfactory stimulation of AWCs provokes cell-nonautonomous regulation of ubiquitin-dependent protein degradation and stress resistance in peripheral tissues, including the intestine. A key regulator of this food response is the Toll-receptor-domain protein TIR-1, which is dynamically regulated by direct binding between *tir-1* mRNA and miR-71 (miR-71–*tir-1*) in AWC neurons. Absence of olfactory information (food odour) or abrogation of post-transcriptional regulation via miR-71 results in elevated *tir-1* levels. Chronic upregulation of *tir-1* in AWC neurons in *mir-71(n4115)* worms alters diet-evoked communication and blocks adjustment of intestinal proteostasis, which correlates with decreased stress tolerance and lifespan.

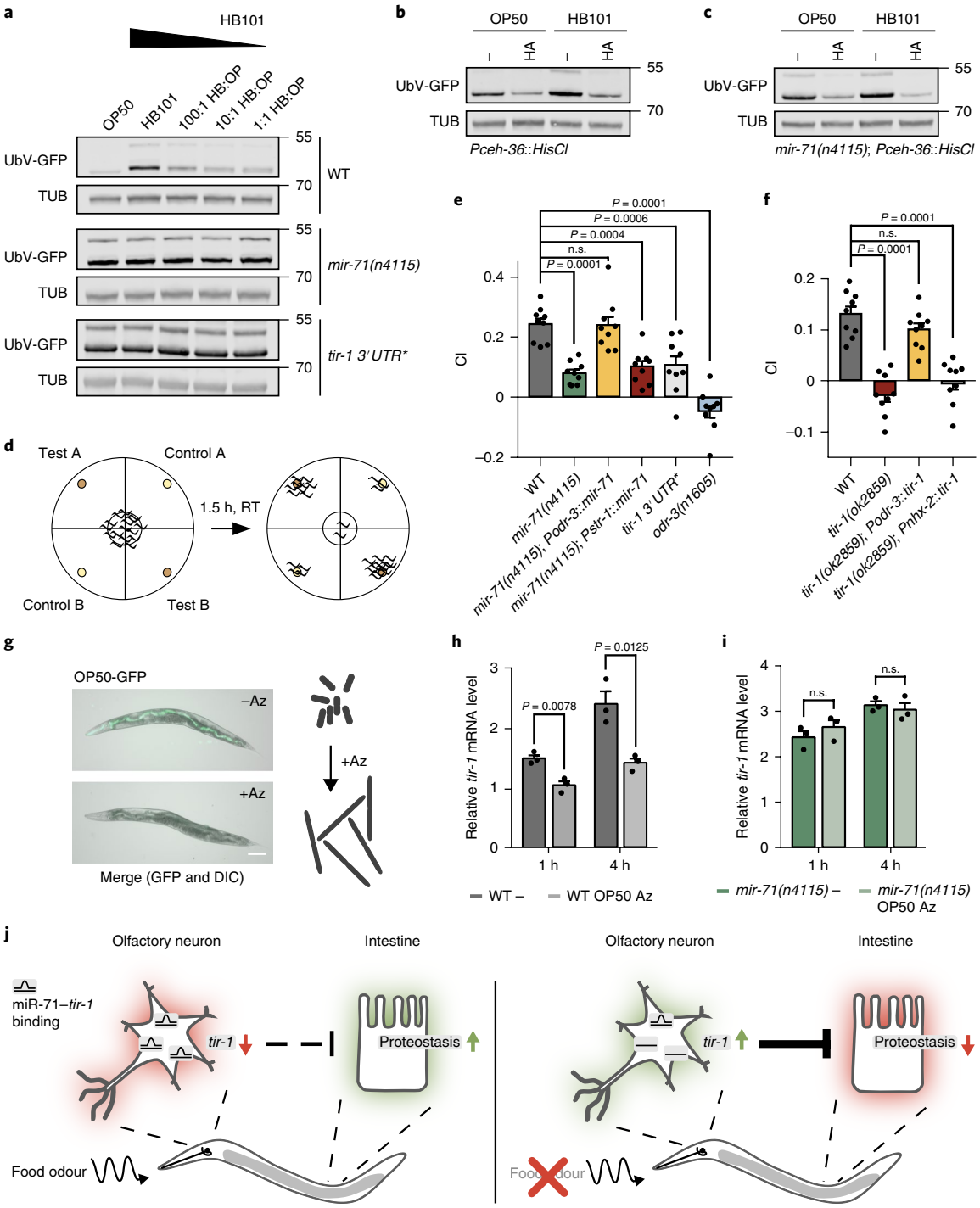

worms fed with HB101 show lower fat storage than those fed OP50, a result indicative of diet-evoked metabolic changes[38]. Along these lines, sense of smell affects metabolic status, especially in the context of obesity and fat storage in mice[39], and regulates the production of digestive enzymes in humans[40]. Our observations show that food source affects intestinal proteostasis[5] (Figs. 3a and 4a, and Supplementary Fig. 5a,b), thus further suggesting a direct link to the metabolic status of the organism. Together, mechanistic insights on organismal control via olfaction might provide a new entry point to control and manipulate diet-related changes in proteostasis and metabolism, with potential implications for associated diseases such as obesity and diabetes.

Methods

***Caenorhabditis elegans* maintenance and transgenic lines.** Nematodes were grown at 20 °C (unless stated otherwise) on nematode growth medium (NGM) plates seeded with the bacterial *E coli* strain OP50 as a food source according to standard protocols and methods[41,42]. The N2 Bristol strain served as the wild type. All strains used in this study are listed in Supplementary Table 6. Transgenic strains expressing *Pnhx-2*::*tir-1*, *Podr-3*::*tir-1* and *Pstr-1*::*mir-71* were constructed via PCR amplification of N2 genomic DNA or cDNA (*nhx-2* promoter, 602-bp genomic DNA[43]; *tir-1*, 2,793-bp cDNA; *tir-1 3′UTR*, 587-bp cDNA; *odr-3* promoter, 2,755-bp genomic DNA[44]; *str-1* promoter, 4,000-bp genomic DNA[14]; and premature *mir-71*, 94-bp genomic DNA). Oligonucleotides used in this study are listed in Supplementary Table 7. PCR fragments were cloned into the IR101 (pDEST R4-R3) vector containing a *Prps0*::*hygR*::*mCherry* cassette for selection of transgenic animals. The constructs were particle bombarded into N2 hermaphrodites and

selected as described previously[45]. Microparticle bombardment was done with a Bio-Rad Biolistic PDS-1000/HE with 1/4-inch gap distance, 9-mm macrocarrier-to-screen distance, 28 inches of Hg vacuum and a 1,350 p.s.i. rupture disc. For each bombardment, approximately 1 mg of 1-µm microcarrier gold beads was coated with 7 µg of linearized DNA. The animals were allowed to recover for 1 h at room temperature and were then transferred to 90-mm enriched peptone plates seeded with *E. coli* C600 bacteria. After 3–4 d, 100 µl of hygromycin B (100 mg ml^{-1}), 600 µl of Antibiotic-Antimycotic 1006 (Gibco Life Technologies) and kanamycin (final concentration 50 µg ml^{-1}) were added to each plate to select transgenic animals on the basis of hygromycin B resistance. Approximately 10 d after bombardment, viable animals were screened for mCherry fluorescence. Individuals positive for mCherry were singled out and screened for homozygosity. Strains expressing the UFD substrate (UbV-GFP) were described previously[5].

CRISPR–Cas9 genome editing. CRISPR–Cas9 mutant alleles were generated as previously described[46]. Briefly, approximately 35–40 worms were injected with a mixture containing 50 ng µl^{-1} *Peft-3*::*Cas9sv40*::*nls*::*tbb-2* (ref. [47]), 50 ng µl^{-1} plk111 (*U6prom*::*sgSRNA*)[48], 50 ng µl^{-1} repair templates (Supplementary Table 8) for homology-directed repair, 3 ng µl^{-1} *Pmyo-2*::*mCherry* and 100 ng µl^{-1} of a plasmid expressing a neomycin-resistance cassette (pBCN44 from ref. [49]). Injected F_0 worms were singled out, and stable lines were selected on OP50-seeded NGM plates, containing 400 µg ml^{-1} neomycin (G-418). All surviving F_1 hermaphrodites within each plate were pooled and tested by PCR for the desired event. In the case of the *tir-1 3′UTR** mutant, the introduced mutations were identified by restriction digestion of the PCR product with KpnI. Non-transgenic animals were cloned out to obtain homozygous isolates, and absence of the extrachromosomal array was verified by PCR. All alleles were validated by Sanger sequencing of the respective loci.

Lifespan and survival assays. For lifespan assays, 100 age-synchronized L4 larvae per strain were transferred to fresh NGM agar plates. Day 0 of the lifespan experiment refers to the first day after reaching adulthood. Within the first 7 d, animals were placed on new plates every day to separate them from F_1 animals and to prevent starvation. After entering the post-reproductive phase, worms were transferred only when necessary. Survival was examined daily by checking pharyngeal pumping or avoidance behaviour in response to mechanical stimuli. All lifespan experiments were carried out in two biological replicates at 20 °C. If indicated, NGM agar plates were supplemented with 25 µM fluorodeoxyuridine to prevent embryonic development and egg hatching[50]. Statistical details for all lifespan experiments are presented in Supplementary Table 1. To dissect sensitivity to ER-stress conditions, NGM plates were supplemented with 50 µg ml^{-1} tunicamycin (an equal amount of DMSO served as a solvent control), and survival was monitored as described above. For proteasome inhibition, NGM agar plates were supplemented with 10 µM BTZ, and L4 larvae were placed on the respective plates. Survival was determined for three consecutive days. Experiments were performed with 50 worms each for three biological replicates. Heat stress was induced by incubation of age-synchronized L4 larvae at 32.5 °C for 15 h. Survival was analysed in three biological replicates with 50–100 worms for each replicate.

Western blotting. For preparation of whole-worm lysates, 100 animals were collected in 80 µl of 1× SDS loading buffer. Subsequently, the samples were boiled at 95 °C for 5 min, sonicated (30 s at 60% amplitude) and again boiled at 95 °C for 5 min. The samples were centrifuged at 15,000 r.p.m. for 5 min. For western blotting, protein lysates were resolved by SDS–PAGE with NuPAGE 4–12% Bis-Tris SDS gels with the respective NuPAGE MES SDS running buffer (Thermo Fisher Scientific; settings according to the manufacturer's instructions). A semidry blotting system (Bio-Rad, Trans-Blot Turbo) was applied with NuPAGE transfer buffer. Antibodies were diluted in 1× Roti-Block (Carl Roth). The following antibodies were used in this study: mouse monoclonal anti-alpha-tubulin (clone B-5–1–2) (Sigma-Aldrich, T6074; RRID:AB_477582), Living Colors Monoclonal Antibody (JL-8) (mouse anti-GFP) (Clontech, 632380) and donkey anti-mouse IRDye 800CW/680 (LI-COR, 926–32212; RRID:AB_621847). Visualization of fluorescent signals was achieved with an Odyssey scanner (LI-COR) and Image Studio Lite v4.0 software. Images of all uncropped blots are shown in Supplementary Fig. 6.

Microscopy. For fluorescence and DIC images, an M165 FC stereomicroscope with a DFC 340 FX camera (Leica Camera) or an Axio Zoom V16 microscope with an Axiocam 506 mono camera (Carl Zeiss Microscopy) was used, and images were processed with Zen 2.3 pro software (Carl Zeiss Microscopy). For close-up images of the *C. elegans* head region, a Confocal Laser Scanning Microscope Zeiss Meta 710 (Carl Zeiss Microscopy) was used. To paralyse worms for imaging, we treated animals with 10 mM levamisole (Sigma-Aldrich) or 60 mM sodium azide (Carl Roth). For analysis of TIR-1::GFP levels in AWC neurons, age-synchronized L4 larvae of *tir-1*::*GFP* worms, also expressing RFP from an AWC-specific promoter (*Podr-1*::*RFP*), were grown until reaching day 1 of adulthood on OP50-seeded NGM plates supplemented with 25 µM BTZ or on plates supplemented with an equal volume of DMSO as a solvent control. Worms were prepared as described above for confocal microscopy, and the obtained images were processed in ImageJ 1.52b. GFP fluorescence intensity was analysed with Imaris 9.l.2 software. Therefore, the volume of AWC neurons was determined in µm^3 by creating a region of interest (ROI) based on RFP fluorescence with a threshold of 0.9 for background subtraction. Within this ROI, the GFP intensity was calculated as fluorescence intensity per cubic millimeter.

RNA interference. RNAi was performed via the feeding method established for *C. elegans*[51,52]. Age-synchronized worms were transferred to RNAi plates seeded with *E. coli* HT115 bacteria expressing the respective double-stranded RNA (dsRNA). Clones carrying the vector against a gene of interest were taken from either the RNAi Collection (Ahringer) (Source BioScience, 3318_Cel_RNAi_complete) or the ORF-RNAi Resource (Vidal)[53] (Source BioScience, 3320_Cel_ORF_RNAi). As a control condition, bacteria transformed with the empty pPD129.36 vector were used for feeding. To achieve enhanced RNAi efficiency in neuronal tissues, additional knockdown of the RNase T enzyme ERI-1 was performed as previously described[54]. Here age-synchronized worms were first fed HT115 bacteria expressing *eri-1* dsRNA for 36 h and then were transferred to RNAi plates with HT115 bacteria expressing both *eri-1* dsRNA and the dsRNA of interest for an additional 36 h. Assessment of phenotypic changes and/or analysis via western blotting was performed at day 1 of the adult stage (approximately 72 h after L1 synchronized worms were placed on RNAi plates).

RNA purification and quantitative real-time PCR. Isolation of total RNA was performed with TRIzol (Invitrogen) and a Qiagen RNeasy kit. Age-synchronized worms were washed twice with M9 buffer, resuspended in 1 ml of TRIzol reagent, and frozen at −80 °C for at least 1 h. Worms were homogenized by the addition of silica beads and subjected to tissue disruption with a Precellys 24-Dual cell homogenizer (Peq-Lab). Next, 1-bromo-3-chloropropane was added to the samples, which were then vigorously mixed and subjected to phase separation via centrifugation. The aqueous phase was used to isolate total RNA with an RNeasy Mini kit (Qiagen) according to the manufacturer's instructions. cDNA synthesis was performed with 200 ng of total RNA with a High-Capacity cDNA Reverse Transcription kit (Applied Biosystems). Gene expression levels were measured via quantitative real-time PCR with Brilliant III Ultra-Fast SYBR Green QPCR Master Mix (Agilent Technologies) and a Bio-Rad CFX96 Real-Time PCR Detection System. For each sample, three technical replicates were analysed, and *cdc-42* and *pmp-3* were used for normalization[55].

Microarray analysis and RNA sequencing. Expression profiling of *mir-71* mutants versus wild-type worms was done with an Affymetrix *C. elegans* Gene Array 1.0. To this end, total RNA of approximately 200–300 age-synchronized day 1 adult hermaphrodites was extracted as described above. Microarray analysis was performed on four replicates per strain and was processed by the Cologne Center for Genomics (CCG). Further quality control (analysis of RNA integrity number (RIN)) and gene expression profiling were performed. The obtained data were analysed in detail with Partek Genomic Suite 6.6. After robust multi-array average (RMA) normalization, one-way ANOVA was performed to identify significant changes. Genome-wide transcriptional responses to proteotoxic stress were analysed by RNA sequencing. Mid-L4-staged N2 worms were placed on OP50-seeded NGM plates containing 25 µM cadmium, 200 µM fluphenazine, 200 µM cantharidin or 10 µM or 25 µM BTZ, and then collected for total RNA extraction with a mirVana microRNA isolation kit (Ambion). Worms treated with *rpn-6.1* RNAi were placed on RNAi plates from early L3 stage on and collected as day 1 adults. For each condition, triplicates of ~2,000 worms each were used for total-RNA extraction. RNA quality control, library preparation of poly(A)-selected transcripts and subsequent Illumina sequencing were conducted by the CCG. Raw data were analysed by the in-house Bioinformatics facility, and fragments per kilobase of exon per million reads mapped (FPKM) were calculated in Cufflinks, and fold changes were computed relative to untreated N2 worms. Significant changes were identified by ANOVA. Filtering of the data and heat-map generation were done in Microsoft Excel. During establishment of the conditions, the various treatments were analysed for their ability to block the proteasome and to induce autophagy. Proteotoxic stress was applied either by fluphenazine- and cantharidin-treatment-induced autophagy or by directly blocking the proteasome with 10 or 25 µM BTZ or *rpn-6.1* RNAi.

Bacterial feeding and chemotaxis assays. To study the effects of different food sources on proteostasis, worms were grown on different bacterial strains, and UFD substrate (UbV-GFP) and *tir-1* mRNA levels were monitored via western blotting and quantitative real-time PCR, respectively. Here age-synchronized L1 larvae were transferred to plates seeded with the respective *E. coli* strain. For inedible food experiments, *E. coli* were treated with the antibiotic Az, which causes cell division stoppage and morphological changes inhibiting subsequent ingestion by *C. elegans*[29,56]. OP50 were grown to log phase at 37 °C, and this was followed by Az treatment (final concentration of 10 µg ml^{-1}) for an additional 3 h at 37 °C and seeding to standard NGM plates 1 d before the experiment. OP50 bacteria expressing GFP (OP50-GFP) were used to control for blocked ingestion after Az treatment (Fig. 4g). Age-synchronized worms were grown until day 1 of adulthood on *E. coli* OP50; transferred to Az-containing plates, control plates or

plates without food; and cultivated for 6 h. The animals were then collected for quantitative real-time PCR as described above.

For studying chemotaxis of *C. elegans*, behavioural assays were adapted from ref. [28]. Chemotaxis studies were performed on freshly prepared agar plates (2% agar, 5 mM KPO_4 (pH 6.0), 1 mM $CaCl_2$ and 1 mM $MgSO_4$). Plates were separated into four equal quadrants (two test and two control quadrants). In each of the test quadrants, 20 µl of OP50 bacteria containing 50 mM sodium azide was placed near the rim of the plate. LB medium was used as a control condition. Age-synchronized worms were grown on NGM plates seeded with OP50 bacteria until day 1 of adulthood, rinsed from plates with S-Basal medium and washed three times. Animals were then transferred to the centre of the chemotaxis plate. After the residual S-Basal medium was soaked in, the plates were sealed with parafilm. After a 1.5-h incubation at room temperature, the number of worms in each quadrant was counted. Individuals that did not cross the inner circle were excluded. The chemotaxis index (CI) was determined with the following equation: CI = ((number of animals at test substance) − (number of animals at control substance))/total number of animals.

Silencing of AWC olfactory neurons. For functional silencing of AWC activity[27], synchronized worms carrying *Ex*[*ceh-36*::*HisCl*;*myo-2*::*GFP*] (a gift from T. Ishihara, Kyushu University, Japan)[57] were grown until the L4 larval stage on *E. coli* OP50 or HB101. L4 larvae were transferred to HA-containing NGM plates (10 mM final concentration) or control plates and allowed to grow until day 1 of adulthood, and this was followed by assessment of proteostasis capability with UFD substrate (UbV-GFP) via western blotting.

Statistical analysis. For statistical analysis, GraphPad Prism 5 software was used. A two-tailed paired Student's *t* test or one-way ANOVA with post hoc test was used to analyse the statistical significance of differences in mRNA levels, fluorescence intensity in AWC neurons, chemotaxis and proteotoxic stress assays. Results are given as mean values and s.e.m. For survival assays, significance was determined with the log-rank (Mantel–Cox) test.

Reporting Summary. Further information on research design is available in the Nature Research Reporting Summary linked to this article.

Data availability

The authors declare that the main data supporting the findings of this study are available within the article and its supplementary information files. RNA sequencing and microarray data have been deposited in the Gene Expression Omibus (GEO) with identifiers GSE124178 (RNA sequencing) and GSE124300 (microarray).

Received: 15 October 2018; Accepted: 4 January 2019;
Published online: 18 February 2019

References

1. Taylor, R. C. & Dillin, A. Aging as an event of proteostasis collapse. *Cold Spring Harb. Perspect. Biol.* **3**, a004440 (2011).
2. Krol, J., Loedige, I. & Filipowicz, W. The widespread regulation of microRNA biogenesis, function and decay. *Nat. Rev. Genet.* **11**, 597–610 (2010).
3. de Lencastre, A. et al. MicroRNAs both promote and antagonize longevity in *C. elegans*. *Curr. Biol.* **20**, 2159–2168 (2010).
4. Mori, M. A. et al. Role of microRNA processing in adipose tissue in stress defense and longevity. *Cell Metab.* **16**, 336–347 (2012).
5. Segref, A., Torres, S. & Hoppe, T. A screenable in vivo assay to study proteostasis networks in *Caenorhabditis elegans*. *Genetics* **187**, 1235–1240 (2011).
6. Denzel, M. S. et al. Hexosamine pathway metabolites enhance protein quality control and prolong life. *Cell* **156**, 1167–1178 (2014).
7. Ruggiano, A., Foresti, O. & Carvalho, P. Quality control: ER-associated degradation: protein quality control and beyond. *J. Cell Biol.* **204**, 869–879 (2014).
8. Vilchez, D. et al. RPN-6 determines *C. elegans* longevity under proteotoxic stress conditions. *Nature* **489**, 263–268 (2012).
9. Calfon, M. et al. IRE1 couples endoplasmic reticulum load to secretory capacity by processing the XBP-1 mRNA. *Nature* **415**, 92–96 (2002).
10. Boulias, K. & Horvitz, H. R. The *C. elegans* microRNA *mir-71* acts in neurons to promote germline-mediated longevity through regulation of DAF-16/FOXO. *Cell Metab.* **15**, 439–450 (2012).
11. Hsieh, Y.-W., Chang, C. & Chuang, C.-F. The microRNA *mir-71* inhibits calcium signaling by targeting the TIR-1/Sarm1 adaptor protein to control stochastic L/R neuronal asymmetry in *C. elegans*. *PLoS Genet.* **8**, e1002864 (2012).
12. Hobert, O. Terminal selectors of neuronal identity. *Curr. Top. Dev. Biol.* **116**, 455–475 (2016).
13. Alcedo, J. & Kenyon, C. Regulation of *C. elegans* longevity by specific gustatory and olfactory neurons. *Neuron* **41**, 45–55 (2004).
14. Troemel, E. R., Kimmel, B. E. & Bargmann, C. I. Reprogramming chemotaxis responses: sensory neurons define olfactory preferences in *C. elegans*. *Cell* **91**, 161–169 (1997).
15. Jan, C. H., Friedman, R. C., Ruby, J. G. & Bartel, D. P. Formation, regulation and evolution of *Caenorhabditis elegans* 3′ UTRs. *Nature* **469**, 97–101 (2011).
16. Chuang, C.-F. & Bargmann, C. I. A Toll–interleukin 1 repeat protein at the synapse specifies asymmetric odorant receptor expression via ASK1 MAPKKK signaling. *Genes Dev.* **19**, 270–281 (2005).
17. Liberati, N. T. et al. Requirement for a conserved Toll/interleukin-1 resistance domain protein in the *Caenorhabditis elegans* immune response. *Proc. Natl Acad. Sci. USA* **101**, 6593–6598 (2004).
18. Xie, Y., Moussaif, M., Choi, S., Xu, L. & Sze, J. Y. RFX transcription factor DAF-19 regulates 5-HT and innate immune responses to pathogenic bacteria in *Caenorhabditis elegans*. *PLoS Genet.* **9**, e1003324 (2013).
19. Taylor, R. C. & Dillin, A. XBP-1 is a cell-nonautonomous regulator of stress resistance and longevity. *Cell* **153**, 1435–1447 (2013).
20. Prahlad, V., Cornelius, T. & Morimoto, R. I. Regulation of the cellular heat shock response in *Caenorhabditis elegans* by thermosensory neurons. *Science* **320**, 811–814 (2008).
21. Madison, J. M., Nurrish, S. & Kaplan, J. M. UNC-13 interaction with syntaxin is required for synaptic transmission. *Curr. Biol.* **15**, 2236–2242 (2005).
22. Speese, S. et al. UNC-31 (CAPS) Is required for dense-core vesicle but not synaptic vesicle exocytosis in *Caenorhabditis elegans*. *J. Neurosci.* **27**, 6150–6162 (2007).
23. Li, C. The ever-expanding neuropeptide gene families in the nematode *Caenorhabditis elegans*. *Parasitology* **131**(Suppl.), S109–S127 (2005).
24. Chalasani, S. H. et al. Dissecting a circuit for olfactory behaviour in *Caenorhabditis elegans*. *Nature* **450**, 63–70 (2007).
25. Hobert, O. et al. Regulation of interneuron function in the *C. elegans* thermoregulatory pathway by the *ttx-3* LIM homeobox gene. *Neuron* **19**, 345–357 (1997).
26. Bargmann, C. I. Chemosensation in *C. elegans*. in *WormBook* (ed. The *C. elegans* Research Community) https://doi.org/10.1895/wormbook.1.123.1 (2006).
27. Pokala, N., Liu, Q., Gordus, A. & Bargmann, C. I. Inducible and titratable silencing of *Caenorhabditis elegans* neurons in vivo with histamine-gated chloride channels. *Proc. Natl Acad. Sci. USA* **111**, 2770–2775 (2014).
28. Ward, S. Chemotaxis by the nematode *Caenorhabditis elegans*: identification of attractants and analysis of the response by use of mutants. *Proc. Natl Acad. Sci. USA* **70**, 817–821 (1973).
29. Ben Arous, J., Laffont, S. & Chatenay, D. Molecular and sensory basis of a food related two-state behavior in *C. elegans*. *PLoS One* **4**, e7584 (2009).
30. Libert, S. et al. Regulation of *Drosophila* life span by olfaction and food-derived odors. *Science* **315**, 1133–1137 (2007).
31. Maier, W., Adilov, B., Regenass, M. & Alcedo, J. A neuromedin U receptor acts with the sensory system to modulate food type-dependent effects on *C. elegans* lifespan. *PLoS Biol.* **8**, e1000376 (2010).
32. Inoue, A. et al. Forgetting in *C. elegans* is accelerated by neuronal communication via the TIR-1/JNK-1 pathway. *Cell Rep.* **3**, 808–819 (2013).
33. Essuman, K. et al. The SARM1 Toll/interleukin-1 receptor domain possesses intrinsic NAD^+ cleavage activity that promotes pathological axonal degeneration. *Neuron* **93**, 1334–1343 (2017).
34. Tsvetkov, P. et al. NADH binds and stabilizes the 26S proteasomes independent of ATP. *J. Biol. Chem.* **289**, 11272–11281 (2014).
35. Summers, D. W., Gibson, D. A., DiAntonio, A. & Milbrandt, J. SARM1-specific motifs in the TIR domain enable NAD^+ loss and regulate injury-induced SARM1 activation. *Proc. Natl Acad. Sci. USA* **113**, E6271–E6280 (2016).
36. Pan, Z.-G. & An, X.-S. SARM1 deletion restrains NAFLD induced by high fat diet (HFD) through reducing inflammation, oxidative stress and lipid accumulation. *Biochem. Biophys. Res. Commun.* **498**, 416–423 (2018).
37. Lin, C.-W. & Hsueh, Y.-P. Sarm1, a neuronal inflammatory regulator, controls social interaction, associative memory and cognitive flexibility in mice. *Brain Behav. Immun.* **37**, 142–151 (2014).
38. Brooks, K. K., Liang, B. & Watts, J. L. The influence of bacterial diet on fat storage in *C. elegans*. *PLoS One* **4**, e7545 (2009).
39. Riera, C. E. et al. The sense of smell impacts metabolic health and obesity. *Cell Metab.* **26**, 198–211 (2017).
40. Teff, K. Nutritional implications of the cephalic-phase reflexes: endocrine responses. *Appetite* **34**, 206–213 (2000).
41. Brenner, S. The genetics of *Caenorhabditis elegans*. *Genetics* **77**, 71–94 (1974).
42. Stiernagle, T. Maintenance of *C. elegans*.in *WormBook* (ed. The *C. elegans* Research Community) https://doi.org/10.1895/wormbook.1.101.1 (2006).
43. Miedel, M. T. et al. A pro-cathepsin L mutant is a luminal substrate for endoplasmic-reticulum-associated degradation in *C. elegans*. *PLoS One* **7**, e40145 (2012).
44. Roayaie, K., Crump, J. G., Sagasti, A. & Bargmann, C. I. The G_α protein ODR-3 mediates olfactory and nociceptive function and controls cilium morphogenesis in *C. elegans* olfactory neurons. *Neuron* **20**, 55–67 (1998).

45. Radman, I., Greiss, S. & Chin, J. W. Efficient and rapid *C. elegans* transgenesis by bombardment and hygromycin B selection. *PLoS One* **8**, e76019 (2013).
46. Drexel, T., Mahofsky, K., Latham, R., Zimmer, M. & Cochella, L. Neuron type-specific miRNA represses two broadly expressed genes to modulate an avoidance behavior in *C. elegans*. *Genes Dev.* **30**, 2042–2047 (2016).
47. Friedland, A. E. et al. Heritable genome editing in *C. elegans* via a CRISPR–Cas9 system. *Nat. Methods* **10**, 741–743 (2013).
48. Katic, I. & Großhans, H. Targeted heritable mutation and gene conversion by Cas9–CRISPR in *Caenorhabditis elegans*. *Genetics* **113**, 155754 (2013).
49. Semple, J. I., Biondini, L. & Lehner, B. Generating transgenic nematodes by bombardment and antibiotic selection. *Nat. Methods* **9**, 118–119 (2012).
50. Mitchell, D. H., Stiles, J. W., Santelli, J. & Sanadi, D. R. Synchronous growth and aging of *Caenorhabditis elegans* in the presence of fluorodeoxyuridine 1. *J. Gerontol.* **34**, 28–36 (1979).
51. Timmons, L. & Fire, A. Specific interference by ingested dsRNA. *Nature* **395**, 854 (1998).
52. Kamath, R. S., Martinez-Campos, M., Zipperlen, P., Fraser, A. G. & Ahringer, J. Effectiveness of specific RNA-mediated interference through ingested double-stranded RNA in *Caenorhabditis elegans*. *Genome Biol.* **2**, RESEARCH0002 (2001).
53. Rual, J. F. et al. Toward improving *Caenorhabditis elegans* phenome mapping with an ORFeome-based RNAi library. *Genome Res.* **14**, 2162–2168 (2004).
54. Jadiya, P. & Nazir, A. A pre- and co-knockdown of RNAseT enzyme, Eri-1, enhances the efficiency of RNAi induced gene silencing in *Caenorhabditis elegans*. *PLoS One* **9**, e87635 (2014).
55. Hoogewijs, D., Houthoofd, K., Matthijssens, F., Vandesompele, J. & Vanfleteren, J. R. Selection and validation of a set of reliable reference genes for quantitative *sod* gene expression analysis in *C. elegans*. *BMC Mol. Biol.* **9**, 9 (2008).
56. Potluri, L. et al. Septal and lateral wall localization of PBP5, the major D,D-carboxypeptidase of *Escherichia coli*, requires substrate recognition and membrane attachment. *Mol. Microbiol.* **77**, 300–323 (2010).
57. Kitazono, T. et al. Multiple signaling pathways coordinately regulate forgetting of olfactory adaptation through control of sensory responses in *Caenorhabditis elegans*. *J. Neurosci.* **37**, 10240–10251 (2017).

Acknowledgements

We thank Y. Kohara and the *Caenorhabditis* Genetics Center (funded by the NIH National Center for Research Resources), the Dana-Farber Cancer Institute, Addgene and Geneservice for plasmids, cDNA and strains. We thank A. Segref (University of Cologne, Germany) for sharing unpublished strains and data on brain-to-gut regulation mechanisms. We thank the CECAD Imaging facility for support with confocal microscopy and the Cologne Center for Genomics for microarray analysis and RNA sequencing. This work is supported by grants from the Deutsche Forschungsgemeinschaft (DFG) (CECAD, FKZ: ZUK81/1 and SFB1218) and the European Research Council (ERC-CoG-616499) to T.H. and grants from the Austrian Science Fund (FWF) (W-1207-B09 and SFB-F43–23) and European Research Council (ERC-StG-337161) to L.C.

Author contributions

F.F., F.O. and A.S. designed, performed and analysed the results of the experiments. A.S. and L.P. performed and analysed the results of the RNA-sequencing experiments; T.D. and L.C. established the gene-edited strains. S.M. performed the stress assays. T.H. supervised the design and data interpretation; F.F., F.O. and T.H. wrote the manuscript. All authors discussed the results and commented on the manuscript.

Competing interests

The authors declare no competing interests.

Additional information

Supplementary information is available for this paper at https://doi.org/10.1038/s42255-019-0033-z.

Reprints and permissions information is available at www.nature.com/reprints.

Correspondence and requests for materials should be addressed to T.H.

Publisher's note: Springer Nature remains neutral with regard to jurisdictional claims in published maps and institutional affiliations.

nature research

Corresponding author(s): Prof. Thorsten Hoppe

Reporting Summary

Nature Research wishes to improve the reproducibility of the work that we publish. This form provides structure for consistency and transparency in reporting. For further information on Nature Research policies, see Authors & Referees and the Editorial Policy Checklist.

Statistical parameters

When statistical analyses are reported, confirm that the following items are present in the relevant location (e.g. figure legend, table legend, main text, or Methods section).

n/a	Confirmed	
☐	☒	The exact sample size (*n*) for each experimental group/condition, given as a discrete number and unit of measurement
☐	☒	An indication of whether measurements were taken from distinct samples or whether the same sample was measured repeatedly
☐	☒	The statistical test(s) used AND whether they are one- or two-sided *Only common tests should be described solely by name; describe more complex techniques in the Methods section.*
☒	☐	A description of all covariates tested
☐	☒	A description of any assumptions or corrections, such as tests of normality and adjustment for multiple comparisons
☐	☒	A full description of the statistics including central tendency (e.g. means) or other basic estimates (e.g. regression coefficient) AND variation (e.g. standard deviation) or associated estimates of uncertainty (e.g. confidence intervals)
☐	☒	For null hypothesis testing, the test statistic (e.g. *F*, *t*, *r*) with confidence intervals, effect sizes, degrees of freedom and *P* value noted *Give P values as exact values whenever suitable.*
☒	☐	For Bayesian analysis, information on the choice of priors and Markov chain Monte Carlo settings
☒	☐	For hierarchical and complex designs, identification of the appropriate level for tests and full reporting of outcomes
☒	☐	Estimates of effect sizes (e.g. Cohen's *d*, Pearson's *r*), indicating how they were calculated
☐	☒	Clearly defined error bars *State explicitly what error bars represent (e.g. SD, SE, CI)*

Our web collection on statistics for biologists may be useful.

Software and code

Policy information about availability of computer code

Data collection	Excel, GraphPad Prism, Bio-Rad CFX Manager
Data analysis	Excel, GraphPad Prism, Bio-Rad CFX Manager, Partek Genomic Suite 6.6

For manuscripts utilizing custom algorithms or software that are central to the research but not yet described in published literature, software must be made available to editors/reviewers upon request. We strongly encourage code deposition in a community repository (e.g. GitHub). See the Nature Research guidelines for submitting code & software for further information.

Data

Policy information about availability of data

All manuscripts must include a data availability statement. This statement should provide the following information, where applicable:

- Accession codes, unique identifiers, or web links for publicly available datasets
- A list of figures that have associated raw data
- A description of any restrictions on data availability

The authors declare that the main data supporting the findings of this study are available within the article and its Supplementary Information files. Extra data are available from the corresponding author upon request.

Field-specific reporting

Please select the best fit for your research. If you are not sure, read the appropriate sections before making your selection.

☒ Life sciences ☐ Behavioural & social sciences ☐ Ecological, evolutionary & environmental sciences

For a reference copy of the document with all sections, see nature.com/authors/policies/ReportingSummary-flat.pdf

Life sciences study design

All studies must disclose on these points even when the disclosure is negative.

Sample size	Exact sample sizes are stated in the according figure legends and Supplementary Information. Sample sizes were chosen to detect 1% changes in lifespan and a minimum of 2% for stress and survival assays. For WB analysis 100 individuals per condition were used.
Data exclusions	No data were excluded from the analyses.
Replication	At least three biological replicates with similar outcome were performed for each experiment. Lifespan determination was done two times with 100 individuals each. Exact numbers and statistics are provided in the Supplementary Information.
Randomization	The samples were not randomized.
Blinding	The samples were not blinded.

Reporting for specific materials, systems and methods

Materials & experimental systems

n/a	Involved in the study
☒	☐ Unique biological materials
☐	☒ Antibodies
☒	☐ Eukaryotic cell lines
☒	☐ Palaeontology
☐	☒ Animals and other organisms
☒	☐ Human research participants

Methods

n/a	Involved in the study
☒	☐ ChIP-seq
☒	☐ Flow cytometry
☒	☐ MRI-based neuroimaging

Antibodies

Antibodies used	Mouse Monoclonal anti-alpha Tubulin (Clone B-5-1-2), Sigma-Aldrich, Cat# T6074 RRID:AB_477582 Living Colors® A.v. Monoclonal Antibody (JL-8) (Mouse anti-GFP), Clontech, Cat# 632380 Donkey anti-mouse IRDye® 800CW/680, LI-COR, Cat# 926-32212 RRID:AB_621847
Validation	Validations of primary and secondary antibodies were done by the stated manufacturer's. Detected protein sizes were as expected.

Animals and other organisms

Policy information about studies involving animals; ARRIVE guidelines recommended for reporting animal research

Laboratory animals	The study involved Caenorhabditis elegans strains of various genotypes listed in the provided Supplementary Information.
Wild animals	The study did not involve wild animals.
Field-collected samples	The study did not involve samples collected from the field.